Research Square

Preprints are preliminary reports that have not undergone peer review.
They should not be considered conclusive, used to inform clinical practice,
or referenced by the media as validated information.

Nd-, Ru- and Mo-doped Uranium Nitrides as Spent Fuel Model Materials: Synthesis, Structure and Ambient Condition Oxidation

Pascal Uhlemann
Forschungszentrum Jülich
Marco Cologna
Joint Research Centre
Martina Klinkenberg
Forschungszentrum Jülich
Sami Vasala
Helmholtz-Zentrum Dresden-Rossendorf
Lucia Amidani
Helmholtz-Zentrum Dresden-Rossendorf
Sergei M. Butorin
Uppsala University
Flavia Digiacomo
Joint Research Centre
Jacobus Boshoven
Joint Research Centre
Oussama Mounouar
Forschungszentrum Jülich
Egor Iwaschko
Forschungszentrum Jülich
Maximilian Henkes
Forschungszentrum Jülich
Philip Kegler
Forschungszentrum Jülich
Felix Brandt
Forschungszentrum Jülich
Kristina O. Kvashnina
Helmholtz-Zentrum Dresden-Rossendorf
Giuseppe Modolo
Forschungszentrum Jülich

Gabriel L. Murphy

g.murphy@fz-juelich.de

Forschungszentrum Jülich

Article

Keywords:

Posted Date: November 19th, 2026

DOI: https://doi.org/10.21203/rs.3.rs-11651255/v1

License: This work is licensed under a Creative Commons Attribution 4.0 International License.
Read Full License

Additional Declarations: No competing interests reported.

Nd-, Ru- and Mo-doped Uranium Nitrides as Spent Fuel Model Materials: Synthesis, Structure and Ambient Condition Oxidation

Pascal Uhlemann,[1]* Marco Cologna,[2] Martina Klinkenberg,[1] Sami Vasala,[3,4] Lucia Amidani,[3,4] Sergei. M. Butorin,[5] Flavia Digiacomo,[2] Jacobus Boshoven,[2] Oussama Mounouar,[1] Egor Iwaschko,[1] Maximilian Henkes,[1] Philip Kegler,[1] Felix Brandt,[1] Kristina O. Kvashnina,[3,4] Giuseppe Modolo,[1] Gabriel L. Murphy[1]*

[1]*Institute of Fusion Energy & Nuclear Waste Management (IFN-2), Forschungszentrum Jülich GmbH, 52428, Jülich, Germany*

[2]*European Commission, Joint Research Centre (JRC), Karlsruhe, Germany*

[3]*Institute of Resource Ecology, Helmholtz-Zentrum Dresden-Rossendorf, 01328,*

Dresden, Germany

[4]*The Rossendorf Beamline BM20 at ESRF, The European Synchrotron, CS40220, 38043,*

Grenoble, Cedex 9, France

[5]*Condensed Matter Physics of Energy Materials, X-ray Photon Science, Department of Physics and Astronomy, Uppsala University, 751 20, Uppsala, Sweden*

*corresponding authors: Pascal Uhlemann (p.uhlemann@fz-juelich.de) and Gabriel L. Murphy (g.murphy@fz-juelich.de)

Abstract

Uranium nitride (UN) is an emerging next-generation nuclear fuel, yet a comprehensive understanding of its chemical makeup as irradiated fuel is absent. Herein, representative Nd-, Mo-, and Ru-doped UN model materials of 5, 10 and 20 % mol were synthesised via a carbothermic reduction approach with simultaneous nitridation, to probe the chemical reactivity and resulting ambient condition oxidation stability of key expected fission products and related surrogates that can form within irradiated UN fuel. Analysis is provided by a combination of X-ray powder diffraction, high energy resolution fluorescence detected X-ray absorption near-edge structure spectroscopy, in combination with scanning electron microscopy measurements. Nd is found to form a continuous solid solution up to the doping levels probed, incorporating as Nd^{3+}, but displays non-ideal mixing when applying a Vegard's law interpretation. Mo forms as metallic precipitates (ε-particles), whereas Ru reacts with the UN matrix forming Ru_3U intermetallic precipitates that occur along grain boundaries. Oxidation experiments over 28 days reveal Mo and Ru_3U have no effect upon the oxidation rate of UN. Contrastingly, Nd is found to catalytically enhance the oxidation of UN, where the susceptibility increases with Nd content. The results of the investigation are discussed in the context of experimental literature studies towards creating a holistic picture of irradiated UN regarding the fission product chemical states can occur and how they affect oxidation stability.

Introduction

Uranium nitride (UN) has recently emerged as a promising fuel candidate for deployment in Generation IV nuclear reactors and small modular reactor systems.[1-3] Compared to conventional uranium oxide (UO_2) based fuels, UN provides superior thermal conductivity and density improving both economics and safety of the nuclear reactor.[1] However, unlike UO_2, UN exhibits heightened susceptibility to oxidation when in contact with oxygen and water, leading to its rapid degradation, challenging its safe handling and use.[4] The complexity of this chemical behaviour is further increased during irradiation, as fission products (FPs) accumulate in the fuel matrix, affecting properties and chemical reactivity of resulting UN-based spent nuclear fuel (UN-SNF). This can impede the successful deployment of UN as nuclear fuel for next-generation nuclear reactor systems and accordingly demands thorough investigation.

In order to decipher the complexity of UN-SNF and gain fundamental insight into its properties, a well-defined FP inventory and well understood chemistry is required. In the absence of sufficient SNF data, previous investigations[5-12] have attempted to address this mainly via computational methods like *ab initio* simulations including DFT, predicting a FP behaviour similarly observed with well investigated UO_2 based SNF, that is commonly described by the original Kleykamp's model.[13] According to this original model that has been verified and enhanced,[14-16] there are 5 classes of FP chemistry classes within UO_2-SNF, dividing into the (1) gaseous FPs released from the fuel matrix, insoluble fuel matrix precipitate FPs that are (2) noble metallic or (3) non-metallic ceramic, (4) FPs that are soluble and can be incorporated into the fuel matrix as a complex solid-solution and (5) volatile and semi-volatile FPs that can be readily released during fuel cladding breach.[14,15] In the case of UN, although some similarities can be made from the UO_2 FP model to it, the inherent chemical difference between nitride and oxide

prevents full transferability. Of those that can form a solid-solution with the UN fuel matrix, lanthanide elements are the largest group, where they are predicted to form a solid solution owing to their isostructural relationship of both UN and *Ln*N crystallising in cubic rock-salt type structure of the space group $Fm\bar{3}m$.[5-7,9-12] Noble metals like Ru belong to the metallic precipitate category, (2), within UO_2 based SNF and are commonly referred to as ε-particles.[13] Similar behaviour is predicted for UN-SNF, as nitrides of Ru are not stable under ambient conditions.[5-7,9-12,17] Within UO_2 based SNF other metals like Mo can be observed either to form metallic or non-metallic precipitates, where it was demonstrated that Mo can exhibit both, mainly metallic precipitate with a small portion oxidised to MoO_2 non-metallic precipitate.[13,18] Mo itself is a critical FP in UO_2 based SNF due to its ability to act as an oxygen buffer. Contrastingly, for UN-SNF, simulations predicted that only metallic precipitation of Mo occurs as it does not form stable nitrides under ambient conditions.[5-7,9-12]

Despite the FP inventory of UN-SNF being relatively well predicted by simulation efforts, there is a considerable paucity of follow-up experimental studies and further understanding of how the chemistry of FPs influences the oxidation behaviour of UN-SNF. Such investigations are necessary considering the known limitations of simulations on actinide bearing materials, particularly bearing U.[19-21] The experimental investigation of UN based materials is challenged by their enhanced susceptibility to oxidation and decomposition upon contact with air.[22] This has limited the use to model systems which can enable critical insight into the fundamental behaviour on single effects of chosen FP elements relevant to SNF.[23,24] Such investigation has been performed for Ce-doped UN model systems, which demonstrated an increased oxidation reactivity of the doped material over pure UN due to catalytic influence of Ce, suggesting that UN-SNF will have reduced oxidation resistance in the presence of secondary Ce fission product phases.[25]

Similarly, Zr solid solutions with UN were observed to exhibit a reduced onset temperature, suggesting increased oxidation reactivity.[26] However, contrasting the results of experimental investigations, DFT simulations suggest that Zr- and Y-FPs would increase oxidation resistance by improving the chemical stability of a passivating oxide layer.[27] Additionally, recent end member studies investigating the oxidation behaviour of lanthanide nitride secondary fission product phases *Ln*N against pure UN highlighted a discordant oxidation behaviour when contacted to air, where *Ln*N preferably react with atmospheric water contrasting the oxygen mediated oxidation mechanism for UN described by Dell and coworkers.[22,28] Recent thermodynamic comparison of Gibbs energies for oxidation reactions of *Ln*N and UN end member phases support the experimental observations, implying that the presence of *Ln*N FPs, particularly via the formation of a solid solution with UN, could stabilise UN-SNF.[29] The contrasting results of different model system computational and experimental investigations highlight the complexity of the FP chemistry interacting with the UN matrix of UN-SNF, which remains poorly understood and requires further investigation.

Considering the paucity of literature pertaining to the experimental investigation of doped UN materials in the context SNF beyond simulation studies that carry known limitations, it is pertinent to examine the solid solution chemistry of doped UN with notable expected FP elements, particularly potential attenuated oxidation effects arising from incorporation and chemical interactions. Consequently, the following investigation has examined the structure formation and associated ambient condition oxidation stability of doped UN with 5, 10 and 20 mol% dopant additions of Nd, Mo and Ru using a critic acid decomposition route followed by carbothermic reduction with simultaneous nitridation. The dopant elements were chosen as representatives for predicted and dominant FP behaviour categories: Nd is expected to form a solid solution with the

UN matrix and is also a good surrogate for Am,[22,23] Ru is chosen as it is expected to form a metallic precipitate which can enable oxidation buffering of the UN system as seen in UO_2 studies,[30] whereas Mo is chosen given its providence towards the stability of UO_2 oxidation acting also as a buffer whilst also possessing potentially variably chemistry. The synthesised nitride materials were chemically and microstructurally characterised via X-ray powder diffraction (PXRD) and scanning electron microscopy (SEM), respectively. High energy resolution fluorescence detected X-ray absorption near-edge structure (HERFD-XANES) measurements were performed to examine the local chemistry of the dopants and determine specific phase speciation. Oxidation stability studies of the materials were performed via ambient condition (25 ºC) air exposure for 28 days, where the evolution of the structure is followed via PXRD characterisation. Microstructural changes to the bulk material post-oxidation were characterised using consistent SEM analysis. The results of the investigation are discussed in relation to the understanding of FP interaction and chemistry within UN-SNF and their ability to influence oxidation resistance, critical to the handling and disposal of irradiated UN.

Experimental

Synthesis

The synthesis of Nd, Ru, and Mo-doped UN materials was carried out using a citric acid route based carbothermic reduction discussed elsewhere.[31,32] The precursor solution was prepared via mixing of uranyl nitrate solution (494.14 g U/L) with citric acid (Alfa Aesar, 99+%) in a U/citric acid ratio of 2.0, where Nd was introduced as $Nd(NO_3)_3 \cdot 6\,H_2O$ (Thermo Scientific, 99.9%) to aim for Nd contents of 5 mol%, 10 mol% and 20 mol% in the final nitride material. A sample batch without Nd was prepared as reference material for comparison. After mixing, the solutions were transferred into alumina (Al_2O_3) crucibles and pyrolysed in argon atmosphere at 1000 °C.[31]

From the pyrolysis UO_2/C nano powder precursors were received that were subjected to carbothermic reduction. To prepare the Ru and Mo-doped UN samples, parts of the UO_2/C mixture were mixed with either Ru (Alfa Aesar, 99.9% purity, 44 μm particle size) or Mo (Sigma Aldrich, 99.9+% purity, 2 μm particle size) powder in a ratio to aim for 5 mol%, 10 mol% and 20 mol% in the final nitride material respectively. The carbothermic reduction was performed in a molybdenum metallic furnace (Degussa VSL10/18) using molybdenum crucibles. The samples were heated in flowing nitrogen atmosphere (1 to 2 NL/min) up to a dwell temperature at 1500 °C. Once the temperature was reached the flowing atmosphere was switched to nitrogen-hydrogen gas containing 5 % H_2 (1 to 2 NL/min) and the temperature held for 8 h. After this dwell time the temperature was raised to 1650 °C and held for another 2 h, after which the furnace was cooled to 1350 °C. At 1350 °C the gas was switched to flowing Argon-hydrogen atmosphere containing 6 % H_2 prior to cooling the furnace to room temperature. The heat treatment for all samples was performed twice to increase the purity of the resulting powders, which had a grey colour and where characterised by PXRD. All heat treatments and sample preparations were carried out in gloveboxes at JRC, where all gloveboxes used to handle nitride materials operated with protective nitrogen atmosphere (O_2 < 50 ppm).

Powder X-ray Diffraction

PXRD data was collected on a Bruker D8 diffractometer equipped with a Lynxeye XE-T detector in Bragg–Brentano configuration using CuK$\alpha_{1,2}$ radiation (λ = 1.54184 Å) at room temperature. The powder samples were placed on a thin Vaseline layer on Si-zero background holders closed by an airtight Kapton dome. Measurements were performed in the range of $10° \leq 2\theta \leq 120°$ with a step size of $(2\theta) = 0.01°$ and a counting time of 2 s per step. Data analysis was performed via the Rietveld method as implemented in the program GSAS-II.[33]

Room temperature oxidation studies

Oxidation of pristine nitride samples was carried out by distributing finely ground powders (< 100 μm particle size) on Si zero background PXRD sample holders, that were prepared with a thin layer of Vaseline to fixate the powders. Each sample was precisely exposed to air at laboratory conditions (23 °C, regular air, 40% humidity) and characterised continuously in a 1-day cycle for 28 days via PXRD.

Mass spectrometry

The dopant content of Nd-doped UN samples with theoretical content of 5 mol%, 10 mol% and 20 mol% Nd after their synthesis were analysed using a PerkinElmer NexION 200C inductively coupled plasma mass spectrometry (ICP-MS). Approximately 20 mg of each sample was dissolved in concentrated nitric acid (65%, EMSURE Reag. Ph Eur, ISO, Merck Millipore) and diluted with 1% v/v HNO_3 by a factor of 1:100000. From each sample 4 aliquots were measured for their Nd and U concentration and the results averaged.

Scanning electron microscopy

The morphology and composition of pristine samples were analysed using a Helios 5 Dual Beam focused ion beam scanning electron microscope (ThermoFisher Scientific, Netherlands) equipped with an Octane elect Super Silicon Drift Detector (EDAX, Weiterstadt, Germany). The powders were distributed on carbon-based sample holders inside of a glovebox under protective Ar atmosphere and individually placed in a transfer shuttle (ThermoFisher Scientific, Netherlands), in which the samples were transferred to the SEM excluding air contact. Backscattered electron (BSE) and secondary electron (SE) images as well as EDS spot measurements and elemental mappings were collected at 20 kV and 1.6 nA at a working distance of 4 mm.

Morphology and composition of oxidised samples were analysed using an Apreo 2 C LoVac scanning electron microscope (ThermoFisher Scientific, Netherlands) equipped with an Octane elect PLUS Silicon Drift Detector (EDAX, Weiterstadt, Germany). The powders were distributed on carbon-based sample holders after 28 days of oxidation without any further treatment. BSE and SE images as well as EDS spot measurements and elemental mappings were collected at 20 kV and 1.6 nA at a working distance of 10 mm.

High energy resolution fluorescence detected X-ray absorption near-edge spectroscopy

U M_4-edge and L_3-edge, Nd L_3-edge HERFD XANES measurements and Mo- and Ru K-edge XANES were performed at the BM20 ROBL beamline of the ESRF, in Grenoble, France.[34] Finely ground powders of pristine UN and respectively 5, 10 and 20 mol% Nd-, Mo-, and Ru-doped UN samples were prepared under protective atmosphere inside an Ar filled glovebox containing less than 1 ppm of O_2/H_2O and placed in specialised holders. Samples of oxidised UN and respectively 10 mol% Nd-. Mo- and Ru-doped UN were prepared after 28 days of air contact using the same methodology. HERFD XANES spectra were collected at room temperature using an X-ray emission spectrometer equipped with five crystal analysers and a silicon drift X-ray detector in a vertical Rowland geometry,[35] where the incident energy was scanned using a Si(111) monochromator. Si(220) crystal analysers were used to acquire the U M4- and the U L3-edge, while Si(331) crystals were used for the Nd L3-edge. XANES at Mo and Ru K-edges were acquired in total fluorescence yield with a silicon drift detector. Data normalisation was performed using the software package PyMca.[36]

The U M_4 HERFD XANES spectra of pristine UN was calculated within the framework of the Anderson impurity model (AIM) as previously reported.[37,38] In order to extract the spectrum of UN in the HERFD mode, the core-to-core (3d–4f) RIXS map of UN for incident photon energies

was calculated across the U M_4 edge using the AIM approach. The calculated U M_4 HERFD-XANES spectrum of UN is derived as a cut of this map through the maximum of the RIXS intensity at the constant emitted energy and along the incident energy axis. In the AIM calculations, the ground, intermediate and final states of the system were each described by a linear combination of three electronic configurations: $5f^2$, $5f^3\underline{\upsilon}^1$ and $5f^4\underline{\upsilon}^2$ are in the ground state; $3d^9 5f^3$, $3d^9 5f^4\underline{\upsilon}^1$ and $3d^9 5f^5\underline{\upsilon}^2$ are in the intermediate state; $4f^{13}5f^3$, $4f^{13}5f^4\underline{\upsilon}^1$ and $4f^{13}5f^5\underline{\upsilon}^2$ are in the final state. In this context $\underline{\upsilon}$ stands for an electronic hole in the valence-band states. The Slater integrals were reduced to 70% of their *ab initio* Hartree-Fock values to account for the configuration interaction and hybridisation effects, except for G^k(4f,5f) integrals which were reduced to 50% of their *ab initio* Hartree-Fock values. Treated as parameters, the ($\varepsilon_\upsilon - \varepsilon_F$), U_{ff}, U_{fd} and U_{fc} values were taken to be −1.0, 3.0, 3.5 and 3.5 eV, respectively, where ε_υ, ε_F are one-electron energies of the valence band and Fermi levels, U_{ff} denotes the 5f–5f Coulomb interaction, U_{fd} and U_{fc} are the 3d and 4f core hole potentials, respectively, acting on the 5f electron. The hybridisation term (hopping matrix element) between $5f^2$ and $5f^3\underline{\upsilon}^1$ configurations and between $5f^3\underline{\upsilon}^1$ and $5f^4\underline{\upsilon}^2$ configurations in the ground state was taken as $V = 0.6$ eV. The same value of the V parameter was used for intermediate and final states of the RIXS process. The Lorentzian broadening in the intermediate (Γ_m) and final (Γ_f) states of the 3d-4f RIXS process were set to 3.2 and 0.5 eV (full width at half maximum), respectively. As a result, the derived 5f occupancy in the ground state of UN is $n_f = 3.14$ electrons.

Results and Discussion

Pristine UN materials containing 5, 10 and 20 mol% of Nd, Mo or Ru dopants were synthesised via citric acid gel combustion assisted carbothermic reduction with simultaneous nitridation, as previously reported.[31] To investigate the impact of these dopants on the structure and chemistry of UN, thus gaining fundamental insight into FP effects on UN-based SNF, all samples were characterised via PXRD. Resulting diffraction data is plotted in Figure 1 alongside a pure UN reference sample synthesised using the same methodology. The diffraction data of the doped UN materials was further analysed using the Rietveld method, with results of the nitride phase with the largest weight contribution summarised in Table 1. Individual plots of Rietveld profiles and complete refinement results are provided in Supplementary Information Note 1, Figure S1 to Figure S2 and Table S1 to Table S2.

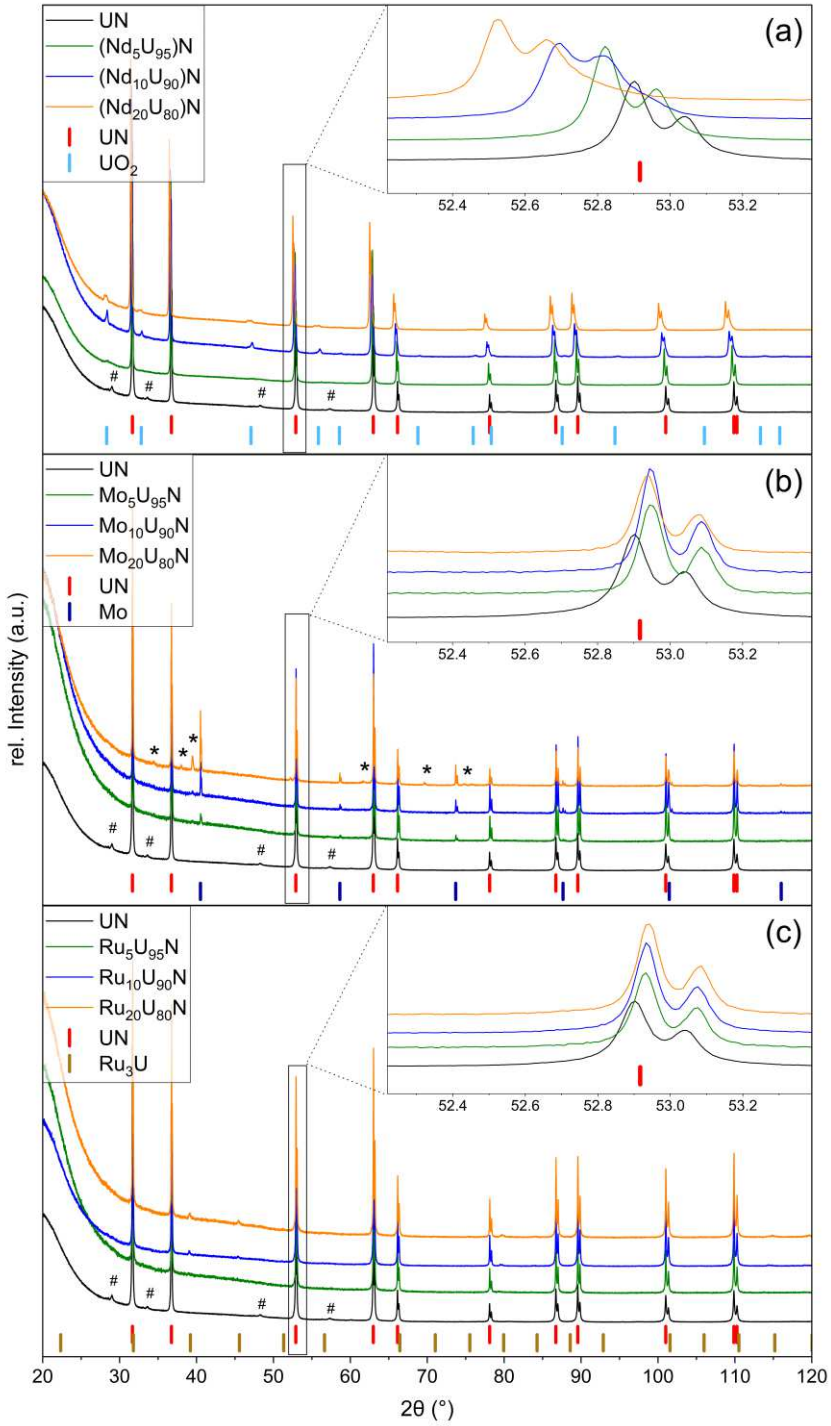


Figure 1. Collected PXRD profiles of UN model materials containing respectively 5 mol, 10 mol and 20 mol% a) Nd, b) Mo and c) Ru plotted against reference pure UN synthesised with similar methodology and setup. Vertical markers represent allowed reflections of literature phases, where red represents UN,[39] light blue UO_2,[40] dark blue Mo,[41] and brown Ru_3U.[42] Secondary impurity phases identified are marked with # for U_2N_3 and * for Mo_2C. The insets provide close up comparison of one chosen reflex position between 52.2° to 53.4° 2θ.

Table 1. Rietveld refinement results for UN model materials containing respectively 5 mol%, 10 mol% and 20 mol% Nd, Ru and Mo dopants. Lattice parameters are given for the identified nitride phase with largest weight contribution based on mass fraction. Additional information about other identified phases and additional refinement parameters are given in Supplementary Information Note 1, Table S1 and S2. Note, uncertainties are quoted directly from refinement analysis and no corrections have been performed.

Model material	Main phase	Space group	Lattice parameter (Å)	Fitting factors (%)	Reference lattice parameter (Å)
UN	UN	$Fm\bar{3}m$ (225)	a = 4.888689(14) (97.3 wt%)	R = 3.60 R_w = 5.64	a = 4.8914(1) [39]
$(Nd_5U_{95})N$	$(Nd_5U_{95})N$	$Fm\bar{3}m$ (225)	a = 4.896338(13) (99.6 wt%)	R = 4.49 R_w = 6.71	
$(Nd_{10}U_{90})N$	$(Nd_{10}U_{90})N$	$Fm\bar{3}m$ (225)	a = 4.906795(20) (69.2 wt%)	R = 3.64 R_w = 5.77	
$(Nd_{20}U_{80})N$	$(Nd_{20}U_{80})N$	$Fm\bar{3}m$ (225)	a = 4.921353(17) (70.4 wt%)	R = 3.18 R_w = 4.83	
$Mo_5U_{95}N$	UN	$Fm\bar{3}m$ (225)	a = 4.889930(15) (92.6 wt%)	R = 4.68 R_w = 8.35	
$Mo_{10}U_{90}N$	UN	$Fm\bar{3}m$ (225)	a = 4.889650(16) (86.4 wt%)	R = 4.93 R_w = 9.13	
$Mo_{20}U_{80}N$	UN	$Fm\bar{3}m$ (225)	a = 4.889126(11) (70.3 wt%)	R = 3.29 R_w = 5.17	
$Ru_5U_{95}N$	UN	$Fm\bar{3}m$ (225)	a = 4.889946(14) (100 wt%)	R = 3.78 R_w = 6.15	
$Ru_{10}U_{90}N$	UN	$Fm\bar{3}m$ (225)	a = 4.890257(17) (97.8 wt%)	R = 6.26 R_w = 10.53	
$Ru_{20}U_{80}N$	UN	$Fm\bar{3}m$ (225)	a = 4.890325(19) (97.0 wt%)	R = 5.55 R_w = 9.91	

Uranium Nitride

The pure reference UN was refined against cubic face centred structure in the space group $Fm\bar{3}m$, isostructural to rock-salt, with a lattice parameter of a = 4.888689(14) Å. Note uncertainties are quoted directly from refinement analysis, without corrections performed. The determined lattice parameter is smaller than the literature reference data of a = 4.8914(1),[39] see Table 1, where the deviation is attributed to non-stoichiometry in the nitrogen content of the synthesised UN sample. Slight U_2N_3 impurities with 2.7 wt% were observed, that were attributed to minimal oxidation during preparation and characterisation of the sample. Although subsequent UO_2 impurities were not detected via PXRD, oxygen hot spots are observed in SEM-EDS elemental mapping that is shown in Figure 2. The overall microstructure of the UN sample has a flaky appearance, that is rounded at the edges and exhibits high porosity. This contrasts the microstructure of bigger solid particles of UN reported recently,[22] where the differing microstructural appearance is attributed to the citric acid gel combustion pre-synthesis step used in this investigation.

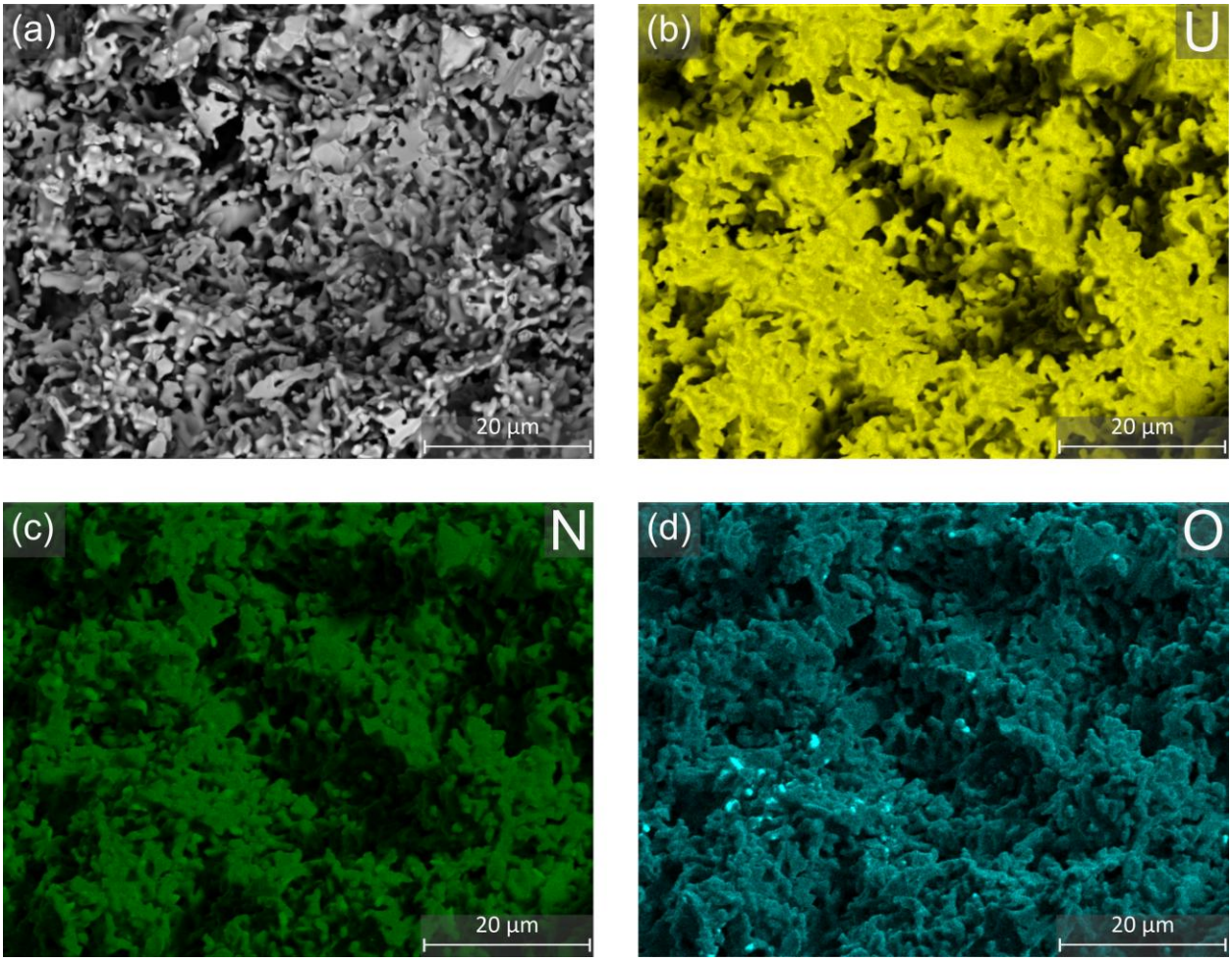


Figure 2. SEM-EDS elemental maps of pristine UN synthesised via citric acid gel combustion assisted carbothermic reduction. (a) BSE image, (b) U-M map, (c) N-K map and (d) O-K map.

HERFD-XANES measurements of UN were performed at the U M_4-edge and at the U L_3-edge, with the resulting spectra compared in Figure 3a and b to a UO_2 reference measured using the same setup and instrument configuration. At both U edges, the UN spectra exhibit post-edge features that differ from those of the UO_2-reference, whereas similarities are observed in the white-line positions and pre-edge regions. The measurements accordingly indicated that some oxidation had occurred to the sample, despite efforts to maintain its purity. In order to better understand how oxidation affects the XAS spectrum of UN, the U_4 XANES and HERFD spectra were calculated with the AIM method for UN, as well as the HERFD spectra for UO_2, where the results of the

calculation are compared in Figure 3 c) against the measured spectra of UN from this study. In comparing the calculated HERFD spectra of the UN and UO_2, very similar pre-edge and white line positions can be observed, but the post edge shows several contrasting features. In particular humps are readily observed for both the UO_2 and UN at non-coincident energies. In the case of the calculated XAS for UN in non-HERFD, these features have significantly lost detail. Noting that this appears to be the first study to provide HERFD measurements of UN, the calculations show that the measured spectra does bear resemblance of UO_2, indicating its presence. However, such features are harder to discern in the calculated XAS spectra, which nevertheless is consistent with previous UN XAS studies that show broadening of such features.[22,43] Moreover, the calculations and experiment show how readily UN can contact oxidation impurities which affect its XANES spectra, of which is harder to discern with normal XANES but become apparent in HERFD. Additionally, this partial oxidation appears to be limited to the surface of the UN sample, as the L_3- post-edge region differs from the UO_2 reference, entirely resembling that of UN recently reported in literature.[22,43]

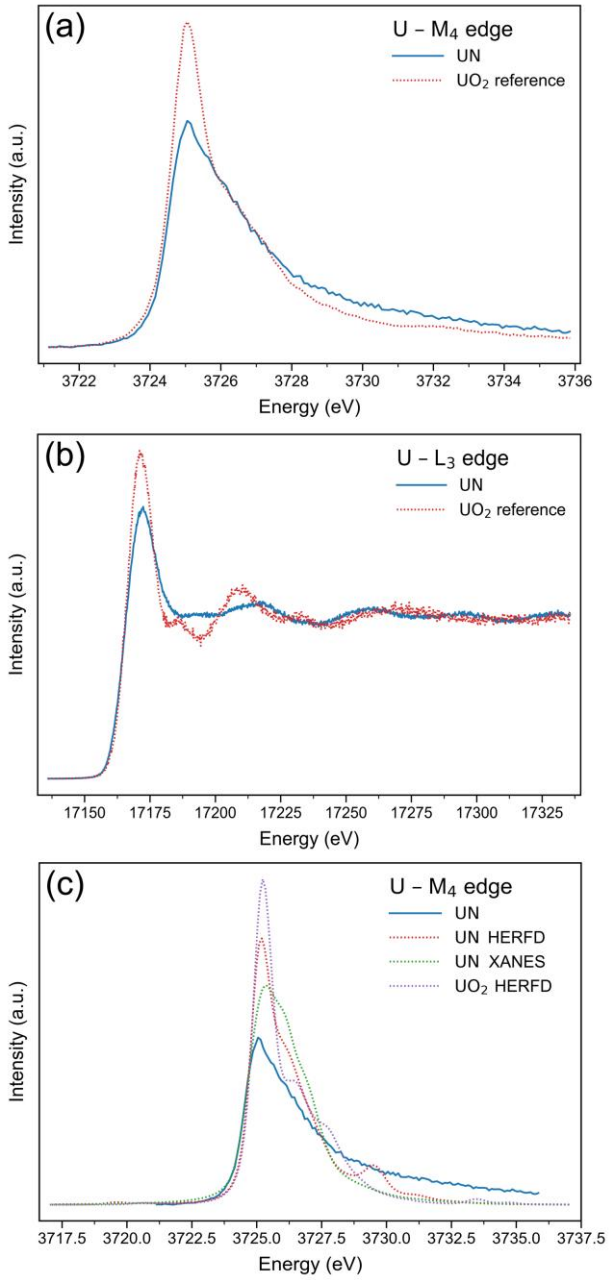


Figure 3. HERFD-XANES spectra of pristine UN synthesised in this investigation. HERFD-XANES spectra normalised to the integrated area of the edges for (a) U M_4-edge in comparison to a UN and UO_2 reference, (b) U L_3-edge in comparison to a UO_2 reference and (c) U M_4-edge in comparison to calculated UN XANES, HERFD and UO_2 HERFD spectra.

Nd-doped Uranium Nitride

From Figure 1a, it is observed that all Nd-doped UN materials show PXRD reflexes which can be attributed to a single-phase structure, which could consistently be refined against cubic rock salt type in the space group $Fm\bar{3}m$ consistent with UN. Comparing the reflex positions, inset Figure 1a, a pertinent trend is observed, where the positions of the reflexes are shifted to lower diffraction angles with increasing Nd content in the material. When the refined lattice parameters from Table 1 are plotted as a function of the Nd content, a linear correlation can be observed, see Figure 4. This behaviour is entirely consistent with solid solution formation.

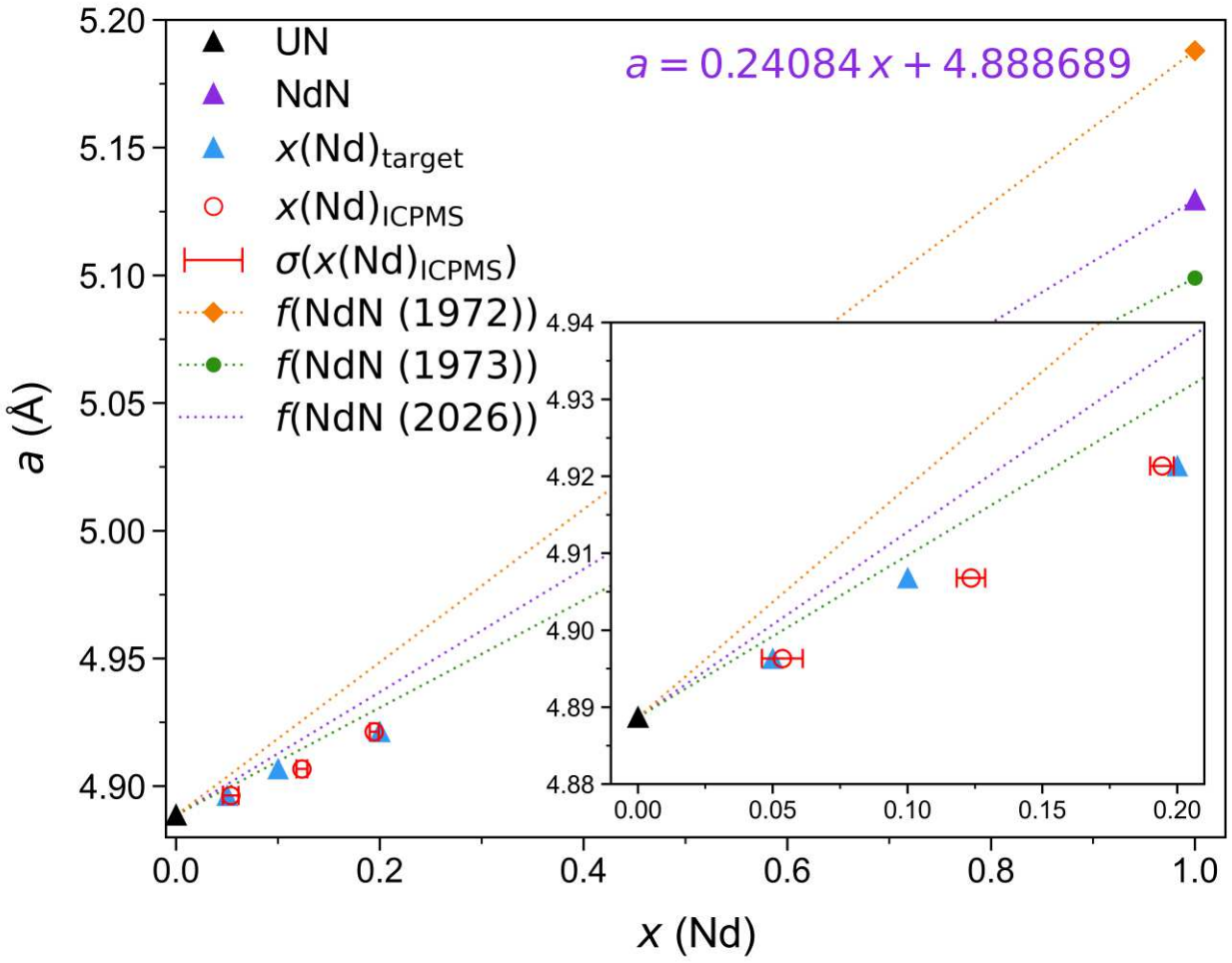


Figure 4. Vegard's law type of lattice parameter determined for UN, NdN from literature,[22,44,45] and Nd-U-N solid solutions investigated against molar Nd content in the sample. Blue triangles mark the Nd contents targeted in synthesis and red dots mark the average

Nd contents in Nd-U-N solid solutions synthesised in this work determined via ICP-MS analysis. Orange, green and violet dotted lines represent Vegard's law functions calculated using literature lattice parameter of NdN marked with orange diamond, violet triangle and green dot symbols.

For a Vegard's law type solid solution a linear trend is expected between isostructural compounds which UN and NdN are.[22,29] Consequently Vegard's law was applied and plotted using the lattice parameter of pure UN from this work and NdN from previously reported investigations.[22,44,45] Since the lattice parameter of nitrides can significantly differ due to varying nitrogen stoichiometry, two other Vegard's law functions were calculated based on the end members utilising different literature lattice parameter of NdN[44,45] and plotted for comparison in Figure 4. When all 3 Vegard's law functions are compared against the lattice parameter trend of the synthesised Nd-U-N solid solution of this study, significant deviation is observed. To verify the Nd contents in the sample were accurate and no Nd loss occurred during synthesis and preparation ICP-MS analysis was performed on synthesized samples. The results are plotted for comparison in Figure 4 as red circles. Molar Nd and U contents were calculated under the assumption of both elements are the only present elements after dissolution in nitric acid. Additional details for the ICPMS analysis are provided in Supplementary Information Note 2, Table S3 and Table S4. The results of ICP-MS characterisation confirm average Nd amounts close to the targeted additions in each Nd-doped UN synthesised material, highlighting a pertinent deviation from ideal Vegard's law type solid-solution. This observation is consistent with previous literature observations of Nd-doped UN and together, strongly indicates non-ideal mixing of Nd in UN as a solid solution.[46,47] In addition to the Nd-U-N solid solutions, minor impurities of UO_2 and U_2N_3 across the samples were identified, which are attributed to oxidation due to contact to air when preparing samples and performing characterisation. For additional details see Supplementary Information Note 1, Figure S1 and Table S2.

Microstructural analysis of 10 mol% Nd-containing UN was carried out using SEM-EDS analysis, where the results are displayed in Figure 5. It can be observed that the overall microstructure consists of fine grains similar to reference UN shown in Figure 2. The formation of UN flakes like in the pristine UN sample is not observed. Nd is largely homogeneously distributed across the sample surface, with some Nd hotspots noticed in the EDS maps Figure 5 c). Moreover, oxygen hotspots resembling oxygen contamination as noticed in PXRD are observed, Figure 5 d). Both the hotspots of Nd and O share positions across the surface of the material, suggesting that oxidation of the doped material is influenced by Nd.

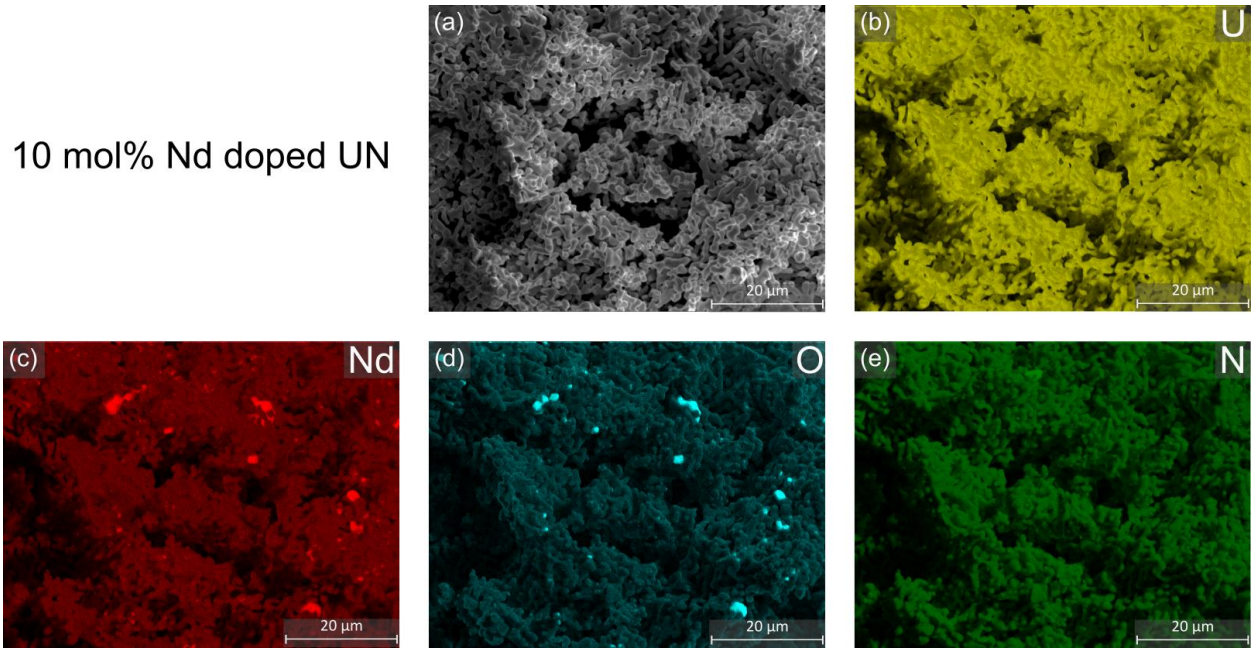


Figure 5. SEM-EDS elemental maps of 10 mol% Nd-doped UN synthesised via citric acid gel combustion assisted carbothermic reduction. (a) SE image, (b) U-M map, (c) Nd-L map, (d) O-K map and (e) N-K map.

HERFD-XANES measurements were performed for all Nd-doped UN samples at the U M_4- and L_3-edge, as well as at the Nd L_3-edge to examine local structural chemical changes arising

from Nd incorporation. The resulting spectra are summarised in Figure 6 and compared with UN, UO_2- and Nd_2O_3-references measured with the same setup and instrument configuration. For comparison, all spectra were normalised to the integrated area of the respective absorption edge.

From Figure 6 a and b it can be observed, that all Nd-doped UN samples exhibit U-edge features and white-line positions closely resembling those of the pristine UN synthesised in this investigation. Moreover, no systematic changes with increasing Nd content are apparent, indicating that Nd incorporation does not significantly alter the chemical state of the UN matrix and that uranium retains its expected +3 oxidation state.[22] Accordingly, incorporation of Nd into the UN lattice is expected to occur predominantly as Nd^{3+}, consistent with its oxidation state in NdN.[22] This assignment is further supported by the Nd L_3-edge spectra in Figure 6 c, for which the white-line positions of all Nd-doped samples are comparable to that of the Nd_2O_3 reference, confirming the presence of Nd^{3+}. Differences in the pre- and post-edge regions between the Nd-doped UN samples and the Nd_2O_3 reference are attributed to the different local chemical environments of Nd in the nitride and oxide compounds.

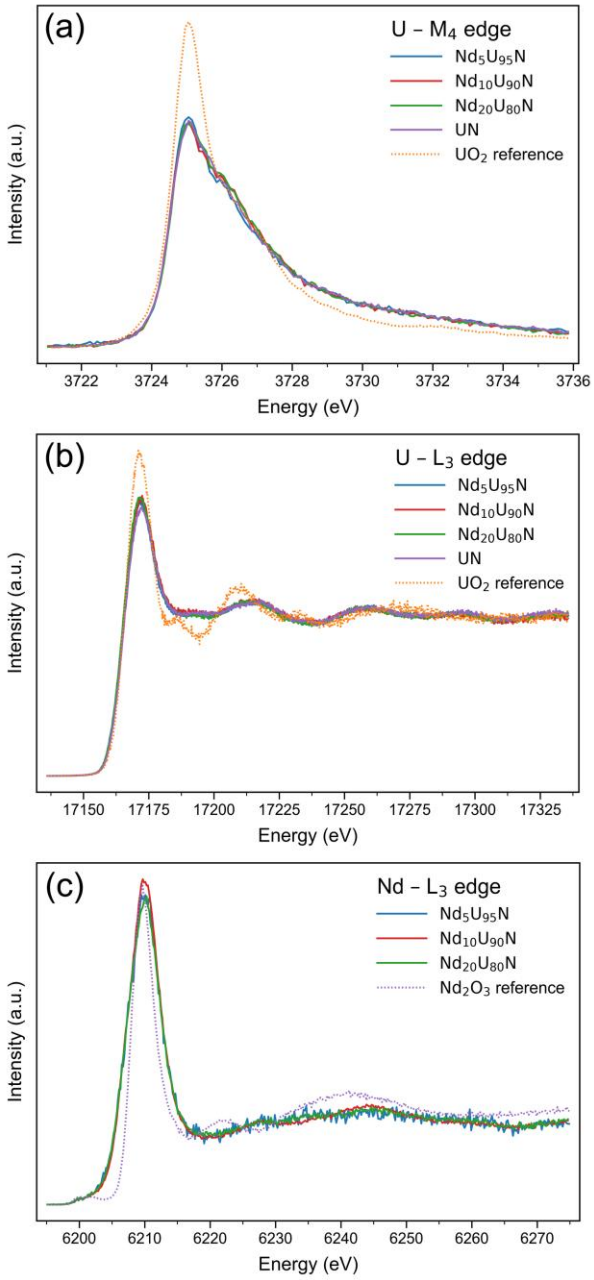


Figure 6. HERFD-XANES spectra of pristine 5, 10, and 20 mol% Nd-doped UN. HERFD-XANES spectra normalised to the integrated area of the edges for (a) U M_4-edge, (b) U L_3-edge in comparison to a UO_2 reference and UN synthesised in this investigation, and (c) Nd L_3-edge in comparison to a Nd_2O_3 reference.

Mo-doped Uranium Nitride

The Mo dopant for each respective sample was introduced as metal powder into the UO_2/C precursor prior to the carbothermic reduction synthesis step. Rietveld analysis revealed that Mo occurs in metallic form, with no other related secondary phases observed, indicating no interaction of Mo with the UN matrix. To investigate this further SEM-EDS analysis on the pristine 10 mol% Mo-doped UN was performed, where the results are displayed in Figure 7. The overall microstructure of the UN matrix matches the flaky microstructure observed in the UN reference shown in Figure 2. Additionally, a clear separation between Mo particles and surrounding UN matrix is observed, which supports no interaction between metallic Mo and UN. Considering Figure 7a, it appears Mo forms as metallic precipitates, precipitating independently from UN which is reminiscent ε-particles that occur in UO_2 SNF.[13,18]

Additionally, minor Mo_2C impurities in the 20 mol% Mo-doped UN were observed, suggesting reaction of metallic Mo with C from the UO_2/C precursor. Noteworthily, despite Mo reacting with carbon from the precursor, no UO_2 impurities were identified in the final materials, that would indicate incomplete carbothermic reduction.

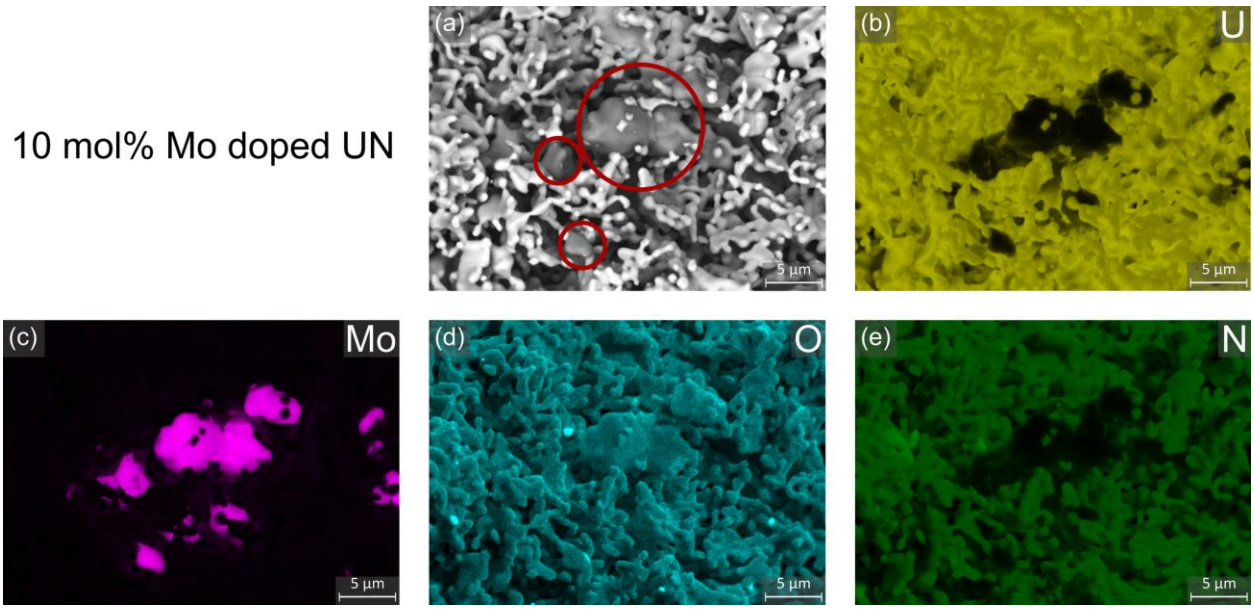


Figure 7. SEM-EDS elemental maps of 10 mol% Mo-doped UN synthesised via citric acid gel combustion assisted carbothermic reduction. (a) SE image, (b) U-M map, (c) Mo-L map, (d) O-K map and (e) N-K map. Red circles mark positions of slightly darker metallic Mo particles in the BSE image which occur as precipitating phases.

To assess the chemical state of Mo in the UN matrix, HERFD-XANES measurements were performed for all Mo-doped UN samples at the U M_4- and U L_3-edges and the Mo K-edge. The obtained spectra were compared with pristine UN synthesised in this investigation, a metallic Mo and oxidic MoO_3 reference, all measured using the same experimental setup and instrument configuration, shown in Figure 8. At the U edges, all Mo-doped samples exhibit white-line positions and pre- and post-edge features comparable to those of pristine UN, suggesting that Mo incorporation does not alter the chemical state of the UN matrix. Similarly, the Mo K-edge spectra closely resemble that of the metallic Mo reference and differ from the MoO_3 reference, supporting the presence of Mo in its metallic state, consistent with the PXRD analysis. These observations are consistent with Mo forming metallic precipitates within the UN matrix rather than being incorporated into the UN matrix as observed via SEM-EDS.

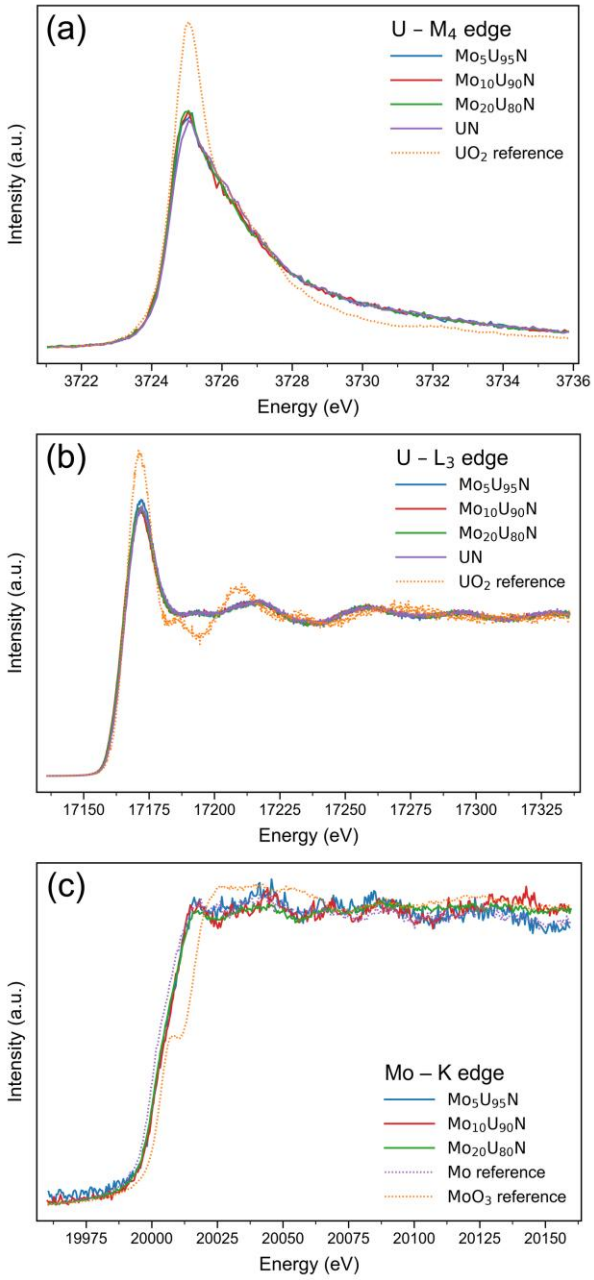


Figure 8. HERFD-XANES spectra of pristine 5, 10, and 20 mol% Mo-doped UN. HERFD-XANES spectra normalised to the integrated area of the edges for (a) U M_4-edge in comparison to UO_2 and UN reference, (b) U L_3-edge in comparison to a UO_2 reference and UN synthesised in this investigation, and (c) Mo K-edge in comparison to a Mo and MoO_3 reference.

Ru-doped Uranium Nitride

Similar to Mo-doped UN model materials, Ru was introduced as metal powder into the UO_2/C precursor prior to carbothermic reduction. Rietveld analysis of the diffraction data shown in Figure 1, shows that Ru formed a Ru_3U intermetallic compound that is found in the diffractogram of 10 and 20 mol% Ru-doped UN. Notably this phase was not observed at the 5 mol% sample, but evidence of phase separation is observed from SEM-EDS analysis discussed further. In PXRD characterisation it is likely not observed due to its low intensity coupled with the PXRD dome holder used in measurement that additionally reduces the intensity of measured phases. In order to form Ru_3U intermetallic compounds within the examined samples, metallic Ru would have to react with the UN matrix directly, particularly extraction of uranium to form Ru_3U and seemingly the loss of N consequently, likely as N_2. This indicates markedly different chemical behaviour than as observed in UO_2-based SNF, where Ru forms as a pure metallic precipitate, which contrasts expectations from simulative investigations of UN-SNF composition.[5-7,9-13,17]

SEM-EDS analysis was performed on pristine 10 mol% Ru-doped UN, with results shown in Figure 9. Noticeably, the overall microstructure is similar to the flaky appearance of reference UN shown in Figure 2. However, unlike the clear separation of dopant and UN matrix noticed for Mo-doped UN, Ru is heterogeneously integrated as particles into the flakes of the UN matrix. A close-up SE picture of the heterogeneous Ru particles is shown in the Supplementary Information Note 3, Figure S3. Further considering Figure 9a shows Ru_3U forming along grain boundaries, suggesting its formation occurs via grain boundary interactions with Ru. Moreover, the results indicate that Ru will interact with the UN matrix, and thus will behave fundamentally different in UN-based SNF compared to its known ε-particle behaviour in UO_2 based SNF.[13] Notably the 5 mol% Ru-doped UN SEM-EDS, Figure S8, show Ru is not incorporating into the UN matrix and

behaving alike the 10 and 20 % mol doped compositions, supporting consistent chemical behaviour.

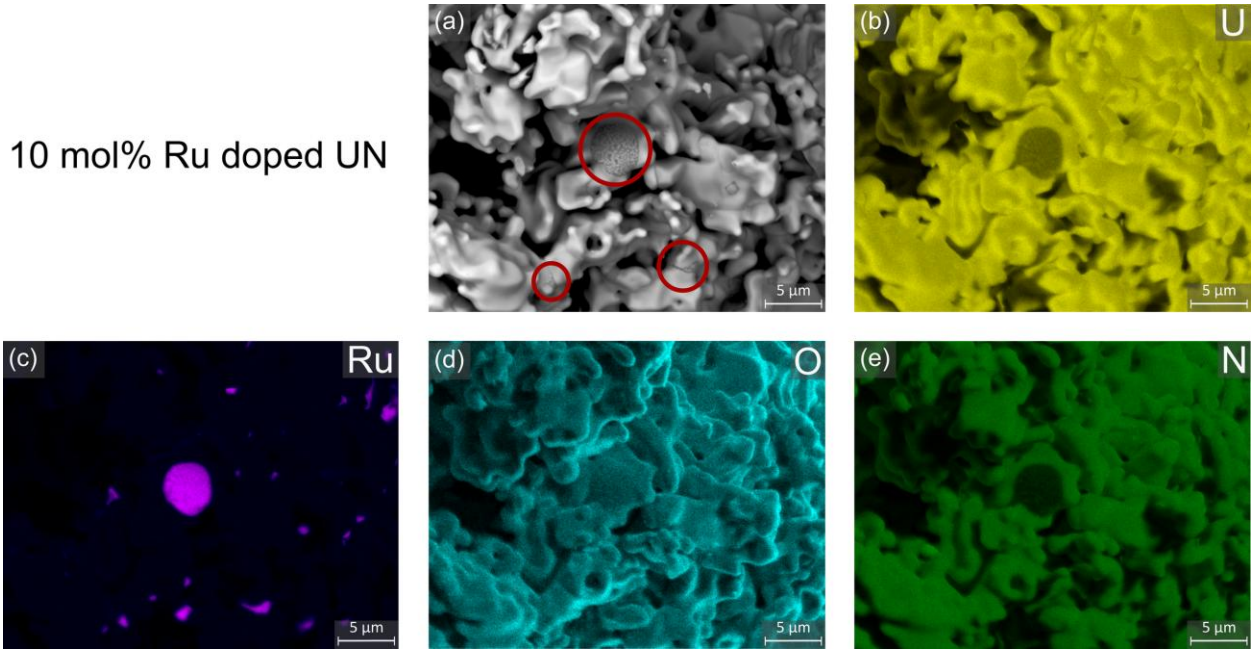


Figure 9. SEM-EDS elemental maps of 10 mol% Ru-doped UN synthesised via citric acid gel combustion assisted carbothermic reduction. (a) BSE image, (b) U-M map, (c) Ru-L map, (d) O-K map and (e) N-K map. Red circles mark position of heterogeneous intermetallic Ru_3U particles appearing predominantly at grain boundaries of UN flakes. A close-up of the heterogeneous particles is provided in Supplementary Information Note 3, Figure S3.

The interaction of Ru with the UN matrix was further investigated by HERFD-XANES measurements at the U M_4- and L_3-edges and the Ru K-edge. The resulting spectra are presented in Figure 10 and compared with pristine UN synthesised in this investigation and a metallic Ru reference, both measured using a similar experimental setup and instrument configuration. It was observed that the Ru-doped UN samples exhibit pre- and post-edge features generally resembling those of the respective reference materials, indicating that the predominant chemical environments of U and Ru remain comparable to those in UN and metallic Ru, respectively for all doping concentrations. However, subtle shifts in the white-line positions relative to the reference materials are observed at all investigated absorption edges. These shifts indicate changes in the local

electronic environments of both U and Ru and are attributed to the interaction between Ru and UN and the subsequent formation of Ru_3U intermetallic precipitates within the UN matrix.

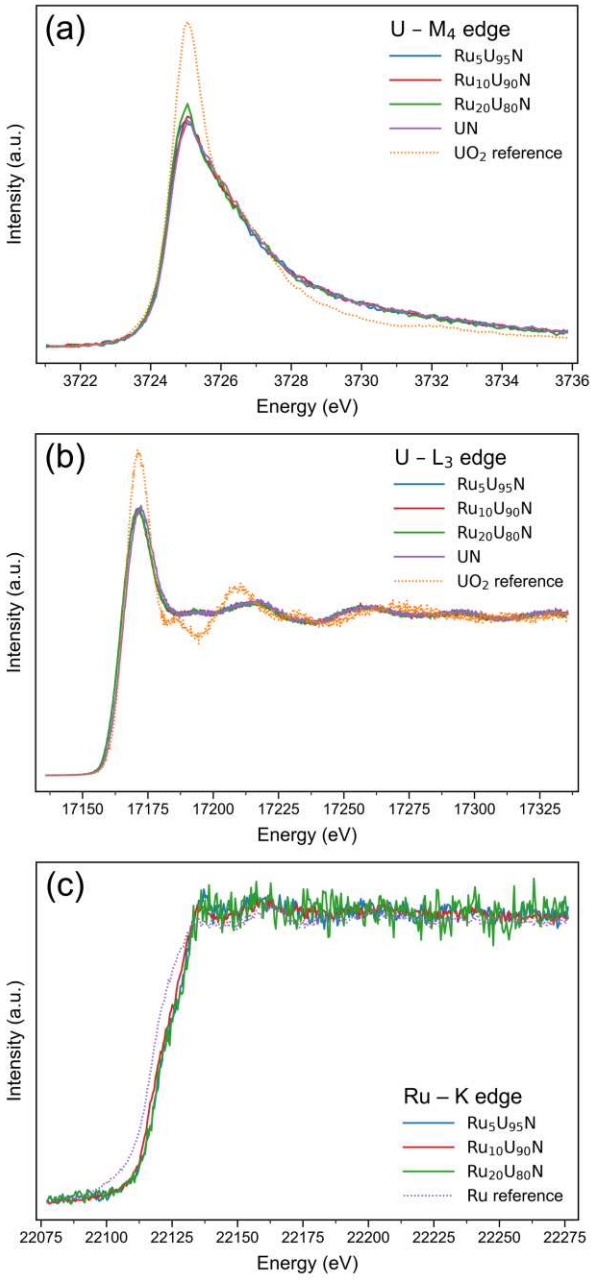


Figure 10. HERFD-XANES spectra of pristine 5, 10, and 20 mol% Ru-doped UN. HERFD-XANES spectra normalised to the integrated area of the edges for (a) U M_4-edge, (b) U L_3-edge in comparison to a UO_2 reference and UN synthesised in this investigation, and (c) Ru K-edge in comparison to a Ru reference.

Oxidation in air at ambient conditions

One of the key challenges with safe handling of UN-SNF, is its susceptibility to oxidise when contacted to atmospheric oxygen and water followed by its subsequent degradation. To investigate this chemical behaviour UN samples containing 5 and 10 mol% Nd-, Mo-, and Ru-doping synthesised in this investigation, were subjected to 28 days oxidation in air at ambient conditions. In this period continuous PXRD characterisation was performed daily to measure the oxidation induced changes to the samples over a 28 days period. Comparison of the received diffraction patterns is displayed in Figure 11 for 10 mol% doped UN materials and in Supplementary Information Note 4 for 5 mol% doped UN materials, highlighting a shift in the reflection positions of the nitride phases to higher 2θ angles. Accordingly, Rietveld sequential analysis was performed, and phases were consistently refined against cubic rock-salt type structure in the space group $Fm\bar{3}m$. The resulting lattice parameters were normalised to the respective Day 1 measurement and are plotted in Figure 12 against the day of the measurement. All samples show consistent contraction of the normalized lattice parameters consistent with oxidation of the samples. Such a contraction of the lattice parameter would be expected during the oxidation of UN to UO_2, as the uranium undergoes a shift from U^{3+} to U^{4+} resulting in a reduction of the ionic radii in a constant 6-fold coordination environment.[48] Moreover, the consistent lattice contraction with air exposure as shown in Figure 11 indicates all samples, UN and Nd-, Mo-, Ru-doped UN, are undergoing oxidation over 28 days but at slightly different rates, discussed below.

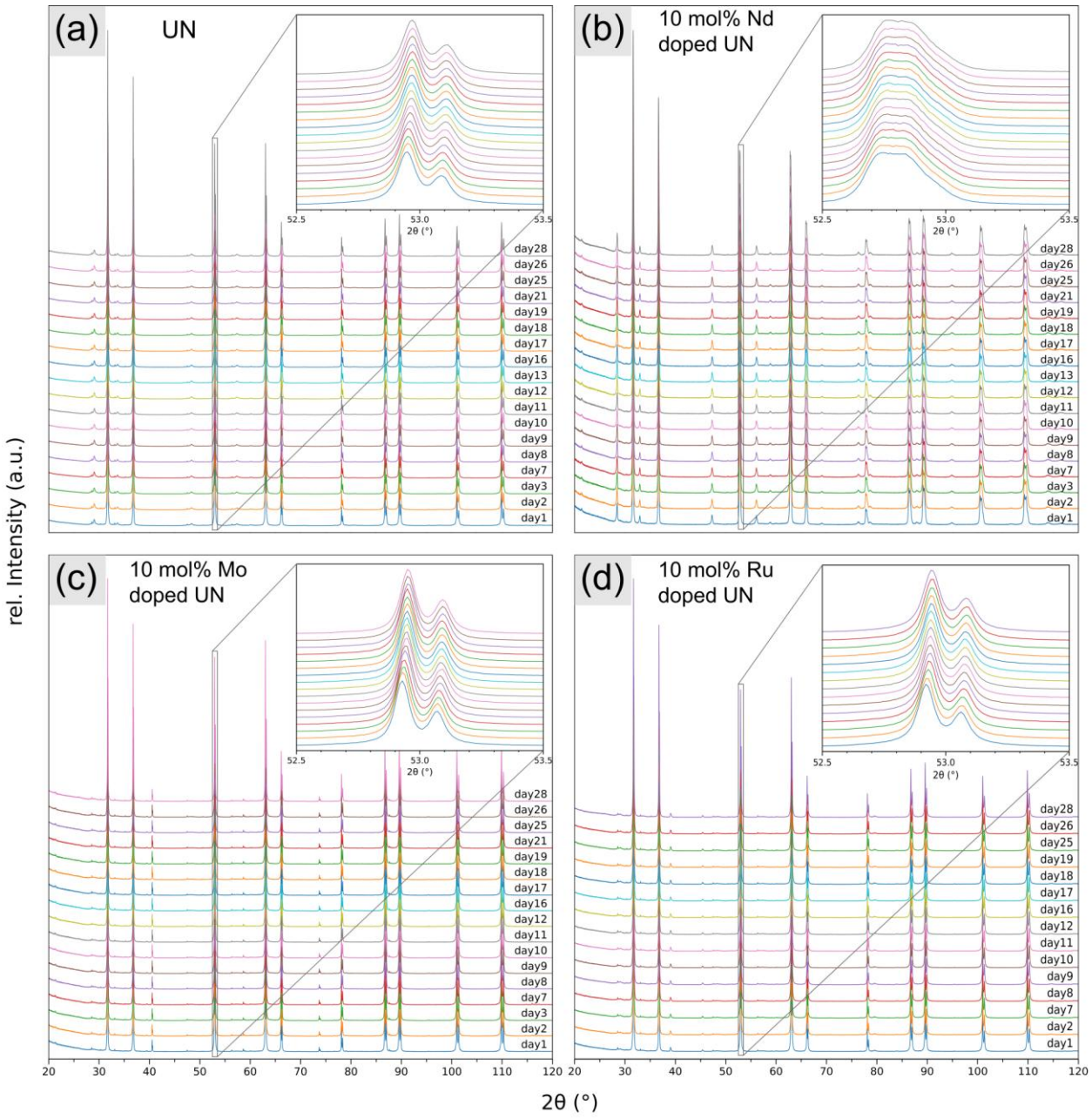


Figure 11. Stacked PXRD data of a) pure UN, b) 10 mol% Nd-doped UN, c) 10 mol% Mo-doped UN and d) 10 mol% Ru doped UN during 28 days of air exposure. Samples were exposed to air for 28 days running a continuous PXRD characterisation every 24 h. Insets provide a close-up comparison shifting reflex positions for identified nitride main phases summarised in Table 1.

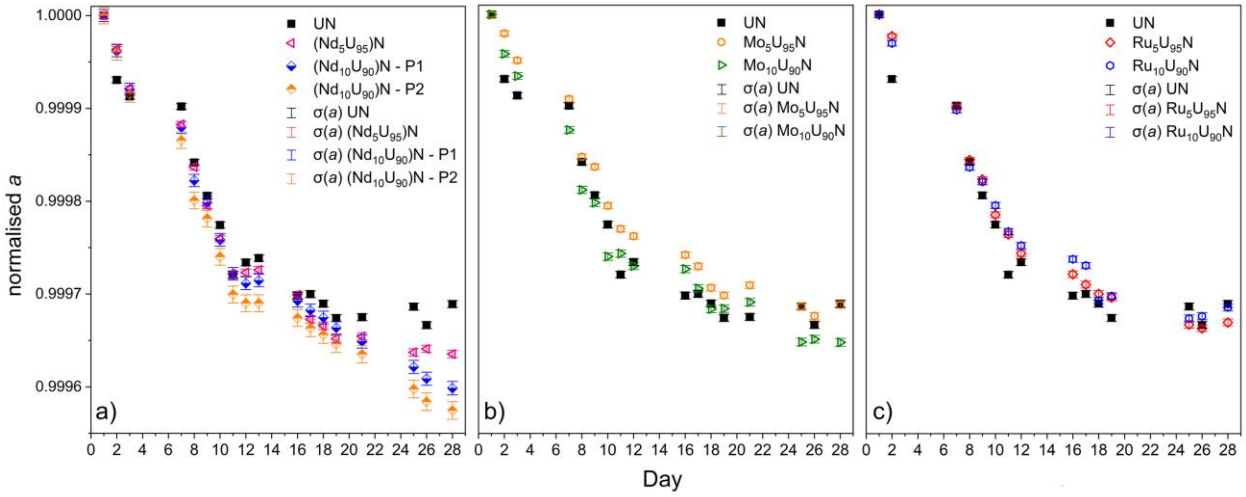


Figure 12. Normalised lattice parameter of main cubic nitride phases of a) Nd-doped UN, b) Mo-doped UN and c) Ru-doped UN against pure UN during 28 days of oxidation via exposure to air at ambient conditions. All compounds were refined against cubic rock-salt type structure in space group $Fm\bar{3}m$.

Figure 12 a) shows the normalised lattice parameter evolution during 28 days of air contact for 5 mol% and 10 mol% Nd-doped UN. It can be observed that after the day 19 measurement, the lattice parameter of the 5 mol% Nd-doped UN samples begins to exhibit a plateau, where the lattice parameter remains constant. Notably, a similar plateau for UN is observed, but appears to begin a few days earlier at day 17. These plateaus indicate that substantial passivation has occurred, which inhibits further oxidation. This chemical behaviour is well known for pure UN, where it was reported that contact to oxygen results in an instantaneously formation of a passivating UO_2 layer followed by a second stage very slow oxidation.[49,50] SEM-EDS analysis performed on the oxidised samples confirmed a surface coverage with oxygen, where images are plotted in Supplementary Information Note 5, Figure S5 and Figure S6.

Noticeably, unlike the 5 mol% Nd-doped UN sample, the lattice parameter of analysed 10 mol% Nd-doped UN phases do not reach a plateau within 28 days of air exposure. This suggests that the oxidation of this sample continues even after 28 days, indicating that Nd at higher contents affect the passivation behaviour of UN, increasing the susceptibility to oxidation. Similar influence

on the oxidation behaviour of UN was reported also for higher contents of 15 mol% and 30 mol% Ce-doped UN.[25] SEM-EDS characterisation of the oxidised 10 mol% Nd-doped UN (Supplementary Information Note 5, Figure S6) revealed that hotspots of oxygen are aggregating on the same positions as Nd, supporting noted influence of Nd on the oxidation behaviour of UN.

Figure 12 b) and c) compares the normalised lattice parameter evolution during air contact respectively for Mo-doped UN materials and Ru-doped materials compared to pure UN characterised as reference. It can be observed that all Mo- and Ru-doped UN materials share similar behaviour compared to that of pure UN, where the lattice parameters exhibit a plateau beginning at day 19 of air exposure. Constant lattice parameters within this plateau suggest passivation of the material, preventing further oxidation. As a result, this indicates that the metals Mo and Ru are barely affecting the oxidation behaviour of UN. SEM-EDS characterisation performed on all samples, for details see Supplementary Information Note 5, Figure S7 and Figure S8, confirm the formation of an oxygen layer across the sample surfaces.

After 28 days of oxidation, the oxidised UN and respectively oxidised 10 mol% Nd-, Mo- and Ru-doped UN samples were further characterised using HERFD-XANES measurements at the U M_4-edge. The resulting spectra were normalised to the maxima of the white line and compared with that of pristine UN in Figure 13, illustrating that no pertinent differences between the pristine UN sample and the oxidised samples of UN, and respectively 10 mol% Mo- and Ru-doped UN samples could be observed. These results support the observation made from the PXRD results, that contact to air results in the formation of a passivating UO_2 layer inhibiting further oxidation. Furthermore, Mo and Ru_3U precipitates within the UN matrix do not interfere with this passivation behaviour. In contrast, the post-edge region of the oxidised 10 mol% Nd-doped UN differs from all other pristine and oxidised samples where it shows a notable shift to higher energy indicating

increased oxidation. Noting that from the PXRD, the original pristine sample already contains oxygen impurities, these measurements indicate an even more enhanced oxidation process is occurring. This observation suggests that the incorporation of Nd into the UN matrix will increase its oxidation and inhibits passivation behaviour, as also observed via PXRD and SEM measurements, thereby reducing the overall oxidation stability of UN.

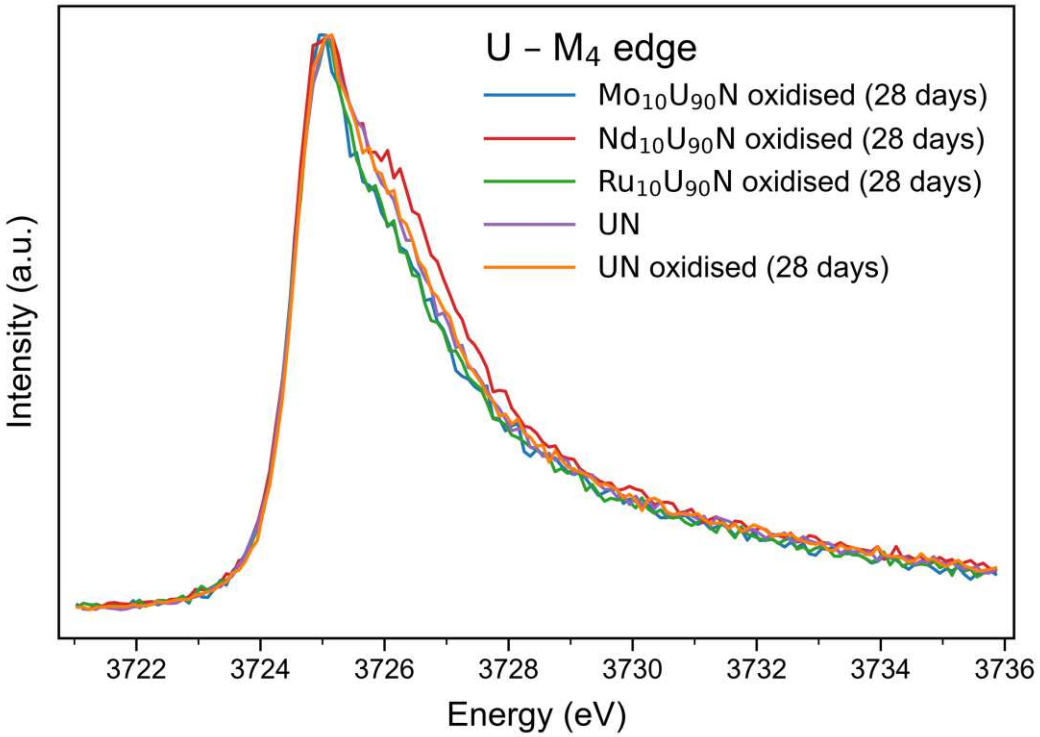


Figure 13. HERFD-XANES spectra of oxidised UN and respectively 10 mol% Nd-, Mo- and Ru-doped UN samples in comparison to pristine UN synthesised in this investigation. Samples were oxidised under ambient conditions via contact to air over a period of 28 days.

Implication for UN-based spent nuclear fuel

This investigation has utilised a model system approach, in which UN was doped with selected Nd, Mo and Ru as surrogate FP elements to examine their individual effects on the chemistry and oxidation stability of UN when occurring as SNF. The investigation reveals that although Nd readily forms a solid solution with UN, it will enhance the oxidation induced degradation of the matrix. Its ability to form a solid solution confirms previous studies that have

argued this.[5,22] Further consistent with previous works,[46,47] it was observed that (Nd, U)N solid solutions deviate from ideal Vegards law type behaviour, suggesting non-ideal mixing despite occurring as $Nd^{3+}$and U^{3+} as shown by XANES analysis in this study. However, oxidation investigations with SEM reveal that Nd will selectively oxidise from the UN matrix rapidly, forming hot spots. Although not investigated in this study, considering previous works, they are likely precipitating as hydroxide like phases.[22] This rapid oxidation of Nd likely acts as a conduit, pulling more atmospheric oxygen with it which then in turn oxidises the bulk UN matrix, whilst at the same time acting as a leak against material layer passivation, allowing oxidation ingress. Comparable effects were also observed for Ce-doped UN, that was described as a catalytic modification of the oxidation mechanism established for pure UN.[25,28] Subsequently, the oxidation of UN brought on by the solid solution with Nd in the present investigation follows a near identical catalytic mechanism. Considering previous studies having shown like chemical and structural behaviour of other lanthanide nitrides (*Ln*N),[22,29] it can be expected that other lanthanides will have a similar effect on the stability of UN in solid solution against oxidation. Consequently, the results of this investigation indicate that for UN based nuclear fuel, increasing fuel burnup with associated increased lanthanide FP accumulation, likely will enhance oxidation susceptibility of UN-SNF.

It is noteworthy that the lanthanide FP behaviour established in this investigation significantly contrasts previously drawn conclusions based on isolated end member investigations of UN and *Ln*N compounds.[22,29] Previous oxidation studies demonstrated that several *Ln*N compounds particularly those containing heavier lanthanide cations, exhibit greater oxidation resistance compared to UN.[22] Subsequent thermodynamic investigation further demonstrated higher oxidation resistance for *Ln*N compounds through a framework constructed utilising Gibbs energies.[29] Consequently, consideration of the oxidation behaviour and thermodynamic properties

of isolated UN and *Ln*N end members suggested a stabilising effect of lanthanide FPs on the UN matrix. In contrast, the results of this investigation demonstrate that incorporation of lanthanides into UN will promote enhanced oxidation catalytically and interfere with the passivation behaviour of the resulting solid solution. This pertinent discrepancy highlights that the chemical behaviour of solid solutions cannot necessarily be extrapolated from the individual end members, as the actual incorporation can affect the local defect chemistry, can cause changes in chemical bonding and influence the microstructure, thereby altering the chemical reactivity. In general, incorporation of dopants can also affect the local electronic structure, although HERFD XANES results obtained for (Nd, U)N solid solutions in this investigation do not support it for the present chemical model system. Consequently, chemical behaviour of UN-SNF cannot be solely predicted from the properties of its individual end members, highlighting the need for representative model systems such as investigated in this study.

Prior to this investigation *in-pile* irradiation studies on mixed (Pu, U)N fuel identified Mo as forming as metallic precipitates.[51] Within UO_2-SNF, Mo is observed to form predominantly metallic ε-particles, while small quantities may occur as MoO_2 depending on the local oxygen potential, which together act as an important oxygen buffer for the fuel.[13,18] Consistent with the aforementioned UN irradiation study, the Mo-doped UN model systems investigated in this study show Mo to form as metallic precipitates. Notably, this highlights that the synthesis method chosen is a good approach to simulate the chemical reactivity and phases that can occur in actual UN-SNF. Moreover, through the absence of chemical or microstructural interaction with the surrounding UN matrix, the influence of Mo on the oxidation behaviour remains limited and rather it is a spectator to such processes and does not appear to offer any kind of oxidation buffer effect.[13,18] However, it should be noted that in actual UN-SNF the chemical behaviour of Mo may

become more complex due to interaction with additional secondary fission product phases that were absent in the model system. For instance, *in-pile* irradiation experiments on mixed (Pu, U)N have demonstrated the formation of mixed Mo-Tc alloys, in which other elements such as U and noble metals like Ru can dissolve.[51]

Unlike the results obtained for Mo-doped UN the results of the Ru-doped UN show a limitation in directly transferring FP behaviour known for UO_2 based SNF onto UN-SNF. Instead of solely forming non-reactive separated ε-particle, Ru in the model materials reacts chemically with the UN matrix to form intermetallic Ru_3U precipitates that are microstructurally incorporated. Considering the chemical similarities between Ru, Rh and Pd and existing Me_3U (*Me* = Ru, Rh, Pd) intermetallic compounds,[11,52] related chemical behaviour may be expected also for other noble metal FP elements, as demonstrated through *in-pile* irradiation experiments on mixed (Pu,U)N fuel.[51] Although the formation of Ru_3U precipitates introduce additional chemical and microstructural heterogeneity into UN-SNF, the results of this investigation suggest their influence on the oxidation behaviour remains limited. During 28 days of air contact Ru-doped UN materials exhibited similar passivation behaviour as observed for pure UN materials, indicating that Ru does not substantially interfere with the oxidation behaviour of UN-SNF.

Inspired by the original chemical model established by Kleykamp describing the UO_2-SNF chemical phase assemblage,[13] the findings of this investigation contribute to the development of a similar periodic-table model summarising the expected chemical behaviour of FPs within UN-SNF shown in Figure 14. Experimental validation of the chemical behaviour was performed in this study for Nd, Mo and Ru FP elements and is therefore displayed as solid colours. Evidence from *in-pile* irradiation experiments further supports these results and extends the experimentally established behaviour to the FP elements Tc, Rh, and Pd, which are indicated by faded colours in

Figure 14.[51] Based on their chemical similarities, the solid-solution behaviour experimentally demonstrated for Nd is further proposed for the remaining lanthanide FPs and minor actinides, represented by a red waved pattern. Although experimental validation remains unavailable for several relevant FP elements, the proposed model provides an important first framework for systematically describing their chemical behaviour within UN-SNF.

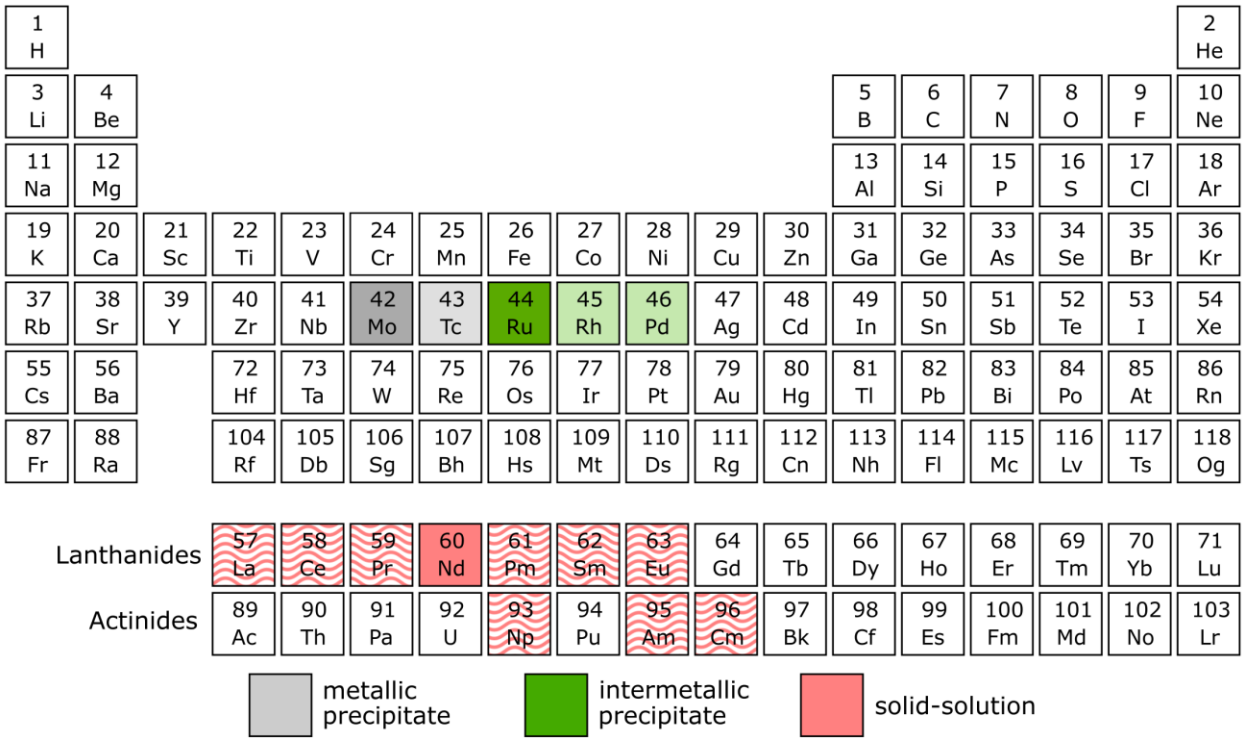


Figure 14. Periodic table of elements marking experimental validated FP behaviour within next-generation UN-SNF. Solid saturated colours mark FP behaviour observed in this investigation. Solid fainted colours mark experimentally validated FP behaviour observed in *in-pile* irradiation experiments.[51] Waved patterns mark chemical behaviour of FPs derived from experimental validated results, based on similar chemistry of the FP elements.

Conclusions

Compounds of UN containing representative Nd-, Mo- and Ru-dopants of 5, 10 and 20 % mol were synthesised using a modified citric acid gel combustion assisted carbothermic reduction with simultaneous nitridation and were investigated regarding structural chemistry and reactivity, in addition to ambient condition oxidation behaviour over 28 days. Combined PXRD and SEM-EDS characterisation revealed Nd forms a complete solid solution up to 20 mol% which can be expected to occur for other lanthanides and minor actinide FPs based on their chemistry and recent investigations[22] in UN-SNF. Non-ideal Vegard's law behaviour was observed, consistent with literature,[46,47] despite XANES measurements showing Nd occurs trivalent in solid solution. Mo was found to precipitate as metallic ε-particles, where it does not react with the surrounding UN matrix. Contrastingly, Ru was found to react with the UN matrix forming intermetallic Ru_3U precipitates along grain boundaries with presumed production of N_2, likely consistent for other platinum group metals occurring as FPs in UN-SNF when considering noted similar chemical behaviour.[11,52] Ambient condition oxidation studies of synthesized materials over a period of 28 days, demonstrated that Nd incorporation leads to catalytically enhanced oxidation of UN, where it interferes with the passivation behaviour of UN, reducing overall oxidation resistance of the material. This effect was found to increase with Nd content, suggesting enhanced oxidation susceptibility of UN SNF at higher burnups. In contrast, Mo- and Ru-containing model systems exhibited oxidation behaviour comparable to pristine UN. The findings of this investigation provide key fundamental insight into the chemical nature of fission product phases forming within irradiated UN and how they contribute to its overall oxidation stability.

Acknowledgments

Financial support for this research was provided by European Commission through the "Fuel Recycle and Experimentally Demonstrated Manufacturing of Advanced Nuclear Solutions for Safety" (FREDMANS) project, grant agreement number 101060800. Views and opinions expressed are those of the author(s) only and do not necessarily reflect those of the European Union, European Commission or European Atomic Energy Community (granting authority). Neither the European Union nor the granting authority can be held responsible for them. Parts of the experimental data used in this research were generated through access to the ActUsLab/FMR under the Framework of access to the Joint Research Centre (JRC) Physical Research Infrastructures of the European Commission (SUNOX, Research Infrastructure Access Agreement N° 37178/04).

Data Availability

The data that support the findings of this study are available from the corresponding author, upon reasonable request.

Conflict of Interest.

The authors confirm they have no conflicts of interest relating to the contents of this publication.

Author Contributions

The research methodology, experimental planning and formal analysis was developed and conducted by **Pascal Uhlemann, Giuseppe Modolo** and **Gabriel L. Murphy**. The materials were synthesised by **Pascal Uhlemann, Flavia Digiacomo**, **Jacobus Boshoven** and **Marco Cologna.** PXRD measurements and analysis were performed by **Pascal Uhlemann** with support and guidance provided by **Philip Kegler**. SEM-EDS characterisation was performed by **Pascal Uhlemann**, **Martina Klinkenberg** and **Felix Brandt**. ICP-MS analysis was performed by **Pascal Uhlemann** and **Maximilian Henkes**.

HERFD-XANES measurements were conducted by **Pascal Uhlemann**, **O. Mounouar**, **E. Iwaschko**, **Gabriel L. Murphy**, **Sami Vasala**, **Lucia Amidani** and **Kristina O. Kvashnina**. Computation of HERFD XANES references was performed by **Sergei M. Butorin**. Manuscript writing, review and editing was performed by **Pascal Uhlemann** and **Gabriel L. Murphy** with input from all authors.

References

1 Kelly, J. E. Generation IV international forum: a decade of progress through international cooperation. *Progress in Nuclear Energy* **77**, 240–246 (2014). https://doi.org:10.1016/j.pnucene.2014.02.010

2 Dehlin, F., Pallarès Abril, E. & Wallenius, J. Performance and safety evaluation of a < 10 wt% ^{235}U enriched small lead-cooled fast reactor. *Annals of Nuclear Energy* **212**, 110861 (2025). https://doi.org:10.1016/j.anucene.2024.110861

3 Dehlin, F., Wallenius, J. & Bortot, S. An analytic approach to the design of passively safe lead-cooled reactors. *Annals of Nuclear Energy* **169**, 108971 (2022). https://doi.org:10.1016/j.anucene.2022.108971

4 Watkins, J. K., Gonzales, A., Wagner, A. R., Sooby, E. S. & Jaques, B. J. Challenges and opportunities to alloyed and composite fuel architectures to mitigate high uranium density fuel oxidation: Uranium mononitride. *Journal of Nuclear Materials* **553**, 153048 (2021). https://doi.org:10.1016/j.jnucmat.2021.153048

5 Degueldre, C., Goddard, D., Berhane, G., Simpson, A. & Boxall, C. Simulation of uranium mononitride spent fuel: A thermodynamic approach. *Journal of Nuclear Materials*, 154900 (2024). https://doi.org:10.1016/j.jnucmat.2024.154900

6 Degueldre, C., Goddard, D. T., Berhane, G., Simpson, A. & Boxall, C. Simulation of uranium mononitride spent fuel: A crystallographic approach. *Journal of Nuclear Materials* **562**, 153612 (2022). https://doi.org:10.1016/j.jnucmat.2022.153612

7 Klipfel, M., Di Marcello, V., Schubert, A., van de Laar, J. & van Uffelen, P. Towards a multiscale approach for assessing fission product behaviour in UN. *Journal of Nuclear Materials* **442**, 253–261 (2013). https://doi.org:10.1016/j.jnucmat.2013.08.056

8 Klipfel, M. & van Uffelen, P. Ab initio modelling of volatile fission products in uranium mononitride. *Journal of Nuclear Materials* **422**, 137–142 (2012). https://doi.org:10.1016/j.jnucmat.2011.12.018

9 Holleck, H. Ternary phase equilibria in the systems actinide-transition metal-carbon and actinide metal-nitrogen. 213–264 (International Atomic Energy Agency, 1974).

10 Arai, Y., Maeda, A., Shiozawa, K.-i. & Ohmichi, T. Chemical forms of solid fission products in the irradiated uranium—plutonium mixed nitride fuel. *Journal of Nuclear Materials* **210**, 161–166 (1994). https://doi.org:10.1016/0022-3115(94)90233-x

11 Uno, M., Kurosaki, K. & Nakamura, A. Reactions of uranium nitride with platinum-family metals. *Journal of Nuclear Materials* **247**, 322–327 (1997). https://doi.org:10.1016/s0022-3115(97)00085-8

12 Holleck, H. & Ishii, T. Berechnung von Gleichgewichten in ternären Systemen Uran-Übergangsmetall-Stickstoff. (Kernforschungszentrum Karlsruhe, Karlsruhe, 1973).

13 Kleykamp, H. The chemical state of the fission products in oxide fuels. *Journal of Nuclear Materials* **131**, 221–246 (1985). https://doi.org:10.1016/0022-3115(85)90460-x

14 Mao, K. S. *et al.* Identifying chemically similar multiphase nanoprecipitates in compositionally complex non-equilibrium oxides via machine learning. *Communications Materials* **3**, 21 (2022). https://doi.org:10.1038/s43246-022-00244-4

15 Colle, J. Y. *et al.* Cesium and iodine speciation in irradiated UO2 fuel. *Journal of Nuclear Materials* **608**, 155715 (2025). https://doi.org:https://doi.org/10.1016/j.jnucmat.2025.155715

16 Piro, M. H. A., Dumas, J.-C., Lewis, B. J., Thompson, W. T. & Iglesias, F. C. in *Comprehensive Nuclear Materials (Second Edition)* (eds Rudy J. M. Konings & Roger E. Stoller) 173-199 (Elsevier, 2020).

17 Cattaruzza, E. *et al.* On the synthesis and thermal stability of RuN, an uncommon nitride. *Surface and Coatings Technology* **295**, 93-98 (2016). https://doi.org:https://doi.org/10.1016/j.surfcoat.2015.10.019

18 Klosek, V. *et al.* Fission product speciation across a UO2 spent nuclear fuel. *Journal of Nuclear Materials* **586**, 154660 (2023). https://doi.org:https://doi.org/10.1016/j.jnucmat.2023.154660

19 Murphy, G. L. *et al.* Tilting and Distortion in Rutile-Related Mixed Metal Ternary Uranium Oxides: A Structural, Spectroscopic, and Theoretical Investigation. *Inorganic Chemistry* **60**, 2246-2260 (2021).

20 Murphy, G. L. *et al.* Pressure induced reduction in SrUO4 – A topotactic pathway to accessing extreme incompressibility. *Acta Materialia* **243**, 118508 (2023). https://doi.org:https://doi.org/10.1016/j.actamat.2022.118508

21 Beridze, G. & Kowalski, P. M. Benchmarking the DFT+ U method for thermochemical calculations of uranium molecular compounds and solids. *The Journal of Physical Chemistry A* **118**, 11797-11810 (2014).

22 Uhlemann, P. *et al.* The Ambient- and High-Temperature Oxidation Behaviour of $U^{3+}N$ and $Ln^{3+}N$ Compounds Relevant to Spent Nuclear Fuel. *npj Materials Degradation* **10** (2026). https://doi.org:10.1038/s41529-026-00827-3

23 Murphy, G. L. *et al.* Structural and chemical insights on the incorporation of americium into zircaloy-derived monoclinic zirconia. *Communications Chemistry* (2025). https://doi.org:10.1038/s42004-025-01857-9

24 McCleary, M. *et al.* Investigating Variable Irradiation Damage Response in Monazite, La1–xLnxPO4 (Ln = Pr, Nd, and Sm) Solid Solution Ceramics. *The Journal of Physical Chemistry C* (2026). https://doi.org:10.1021/acs.jpcc.6c03822

25 Dehadraya, J. V. *et al.* The oxidation of uranium-cerium mononitride microspheres. *Journal of Alloys and Compounds* **257**, 313–321 (1997). https://doi.org:10.1016/s0925-8388(97)00010-8

26 Mishchenko, Y., Patnaik, S., Wallenius, J. & Adorno Lopes, D. Thermophysical properties and oxidation behaviour of the U0.8Zr0.2N solid solution. *Nuclear Materials and Energy* **35**, 101459 (2023). https://doi.org:10.1016/j.nme.2023.101459

27 Yang, S. *et al.* Atomic-scale insights into oxidation of Zr- and Y-doped UN surfaces and grain boundaries in steam: A first-principles study. *Surfaces and Interfaces* **65**, 106490 (2025). https://doi.org:10.1016/j.surfin.2025.106490

28 Dell, R. M., Wheeler, V. J. & McIver, E. J. Oxidation of uranium mononitride and uranium monocarbide. *Transactions of the Faraday Society* **62**, 3591 (1966). https://doi.org:10.1039/tf9666203591

29 Uhlemann, P. *et al.* The Energetics of High Temperature Oxidation and Formation Mechanisms in Binary Lanthanide Nitrides (*Ln*N). *Communications Chemistry* **9** (2026). https://doi.org:10.1038/s42004-026-02236-8

30 Broczkowski, M. E., Noël, J. J. & Shoesmith, D. W. The inhibiting effects of hydrogen on the corrosion of uranium dioxide under nuclear waste disposal conditions. *Journal of*

Nuclear Materials **346**, 16-23 (2005). https://doi.org:https://doi.org/10.1016/j.jnucmat.2005.04.070

31 Bonani, W., Boshoven, J. & Cologna, M. Uranium nitride from uranyl citrate gel combustion and electrospray-assisted granulation. *Journal of Nuclear Materials* **616**, 156036 (2025). https://doi.org:10.1016/j.jnucmat.2025.156036

32 Salvato, D. *et al.* Innovative preparation route for uranium carbide using citric acid as a carbon source. *Ceramics International* **42**, 16710-16717 (2016). https://doi.org:https://doi.org/10.1016/j.ceramint.2016.07.138

33 Toby, B. H. & Dreele, R. B. v. GSAS-II: the genesis of a modern open-source all purpose crystallography software package. *Journal of Applied Crystallography* **46**, 544–549 (2013). https://doi.org:10.1107/s0021889813003531

34 Scheinost, A. C. *et al.* ROBL-II at ESRF: a synchrotron toolbox for actinide research. *Journal of Synchrotron Radiation* **28**, 333-349 (2021). https://doi.org:10.1107/S1600577520014265

35 Kvashnina, K. O. & Scheinost, A. C. A Johann-type X-ray emission spectrometer at the Rossendorf beamline. *Journal of Synchrotron Radiation* **23**, 836-841 (2016). https://doi.org:doi:10.1107/S1600577516004483

36 Solé, V. A., Papillon, E., Cotte, M., Walter, P. & Susini, J. A multiplatform code for the analysis of energy-dispersive X-ray fluorescence spectra. *Spectrochimica Acta Part B: Atomic Spectroscopy* **62**, 63-68 (2007). https://doi.org:https://doi.org/10.1016/j.sab.2006.12.002

37 Butorin, S. M. *et al.* Effect of carbon content on electronic structure of uranium carbides. *Scientific Reports* **13**, 20434 (2023). https://doi.org:10.1038/s41598-023-47579-7

38 Butorin, S. M. *et al.* X-ray spectroscopic study of chemical state in uranium carbides. *Journal of Synchrotron Radiation* **29**, 295-302 (2022). https://doi.org:doi:10.1107/S160057752101314X

39 Liu, J. *et al.* Thermal expansion and steam oxidation of uranium mononitride analysed via in situ neutron diffraction. *Journal of Nuclear Materials* **575**, 154215 (2023). https://doi.org:10.1016/j.jnucmat.2022.154215

40 Desgranges, L., Baldinozzi, G., Rousseau, G., Nièpce, J.-C. & Calvarin, G. Neutron diffraction study of the in situ oxidation of UO_2. *Inorganic Chemistry* **48**, 7585–7592 (2009). https://doi.org:10.1021/ic9000889

41 Bernuy-Lopez, C., Allix, M., Bridges, C. A., Claridge, J. B. & Rosseinsky, M. J. Sr 2 MgMoO 6-δ : Structure, Phase Stability, and Cation Site Order Control of Reduction. *Chemistry of Materials* **19**, 1035–1043 (2007). https://doi.org:10.1021/cm0624116

42 Ott, H. R., Hulliger, F., Rudigier, H. & Fisk, Z. Superconductivity in uranium compounds with Cu3Au structure. *Physical review. B, Condensed matter* **31**, 1329–1333 (1985). https://doi.org:10.1103/PhysRevB.31.1329

43 Goncharov, V. G. *et al.* Energetics of oxidation and formation of uranium mononitride. *Journal of Nuclear Materials* **569**, 153904 (2022). https://doi.org:10.1016/j.jnucmat.2022.153904

44 Kieffer, R., Ettmayer, P. & Pajakoff, S. Über Mononitride und stickstoffreichere Nitride der Seltenerdmetalle (Mitt. I). *Monatshefte für Chemie / Chemical Monthly* **103**, 1285-1298 (1972). https://doi.org:10.1007/BF00904513

45 Schobinger-Papamantellos, P., Fischer, P., Vogt, O. & Kaldis, E. Magnetic ordering of neodymium monopnictides determined by neutron diffraction. *Journal of Physics C: Solid State Physics* **6**, 725–737 (1973). https://doi.org:10.1088/0022-3719/6/4/020

46 Smailos, E. Reactions of fission products in carbide and nitride fuel based on simulated experiments. Report No. KFK 1953, (Kernforschungszentrum Karlsruhe, 1974).

47 Holleck, H., Smailos, E. & Thümmler, F. Zur Mischkristallbildung von UN mit den Nitriden der Seltenen Erden CeN und NdN. *Journal of Nuclear Materials* **28**, 105–109 (1968). https://doi.org:10.1016/0022-3115(68)90061-5

48 Shannon, R. D. Revised effective ionic radii and systematic studies of interatomic distances in halides and chalcogenides. *Acta Crystallographica Section A* **32**, 751–767 (1976). https://doi.org:10.1107/s0567739476001551

49 Ikawa, K. & Taketani, K. Room temperature oxidation of UN powder. *Journal of Nuclear Science and Technology* **7**, 433–438 (1970). https://doi.org:10.1080/18811248.1970.9734717

50 Lawrence Bright, E. *et al.* Oxidation and passivation of the uranium nitride (001) surface. *Corrosion Science*, 110705 (2022). https://doi.org:10.1016/j.corsci.2022.110705

51 Giacchetti, G., Sari, C. & Walker, C. T. Actinides and fission products distribution in fast breeder nitride fuel. *Nuclear Technology* **28**, 216–225 (1976). https://doi.org:10.13182/nt76-a31562

52 Volgin, M. I. *et al.* U(Ru, Rh, Pd)3 mixed intermetallics: Structural features and chemical activity. *Journal of Nuclear Materials* **618**, 156219 (2026). https://doi.org:https://doi.org/10.1016/j.jnucmat.2025.156219

Supplementary Files

This is a list of supplementary files associated with this preprint. Click to download.

- ManuscriptSIUNmodelsystemsdraftFinal.docx